JACS
JOURNAL OF THE AMERICAN CHEMICAL SOCIETY
pubs.acs.org/JACS
Article

The Prototypal Diamondoid Topology Hybrid Ultramicroporous Materials and Their Water Vapor Sorption Properties

Yassin H Andaloussi,[‖] Aizhamal Subanbekova,[‖] Kyriaki Koupepidou, Sousa Javan Nikkhah, Andrey A. Bezrukov, Asif Raza, Hirotoshi Sakamoto, Susumu Kitagawa, Matthias Vandichel, Soumya Mukherjee, and Michael J. Zaworotko*

Cite This: *J. Am. Chem. Soc.* 2025, 147, 46145−46151
Read Online
ACCESS | Metrics & More | Article Recommendations | Supporting Information

ABSTRACT: We report the green synthesis and sorption properties of [Cu(SnF_5OH)(2,2′-bipyrimidine)], **dia-SNIFFOH-1-Cu**, the first hybrid ultramicroporous material (HUM) with diamondoid (**dia**) topology and the first porous material of any class to be comprised of pentafluorohydroxostannate(IV) (SNIFFOH) linker anions. Single crystal and variable temperature powder X-ray diffraction revealed that **dia-SNIFFOH-1-Cu** exhibits reversible single-crystal-to-single-crystal (SC−SC) transformation between its as-synthesized hydrated form (**dia-SNIFFOH-1-Cu-*α***, Cc, V = 1414.45(6)) and a nonporous anhydrous form (**dia-SNIFFOH-1-Cu-*β***, Cc, V = 1240.8(7)) induced by temperature or humidity swing. Dynamic water vapor sorption experiments revealed S-shaped isotherm profiles with an inflection point at ∼10% relative humidity (RH) and uptake of 12 weight-% (313 cm^3/cm^3) at 90% RH. Humidity swing cycling (0−30% RH) indicates hydrolytic stability over at least 50 adsorption/desorption cycles. Notably, whereas H_2O induced this phase transformation, CO_2 (195 and 298 K), He (77 and 298 K), N_2 (77 K), and C_2/C_3 hydrocarbons (298 K) registered negligible uptakes. **dia-SNIFFOH-1-Cu** is to our knowledge the first porous sorbent that can serve as a sieve for water over gases as verified by dynamic breakthrough experiments conducted with wet CO_2. Whereas the pentafluorooxoniobate analog, **dia-NBOFFIVE-1-Cu**, is isostructural (Cc, V = 1178.52(9)) with **dia-SNIFFOH-1-Cu-*β***, it has different pore chemistry that inhibits H_2O adsorption. **dia-SNIFFOH-1-Cu** represents a rare example of a flexible desiccant that, thanks to a low RH step and high volumetric uptake, offers high volumetric productivity for atmospheric water harvesting while also serving as a sieve toward CO_2.

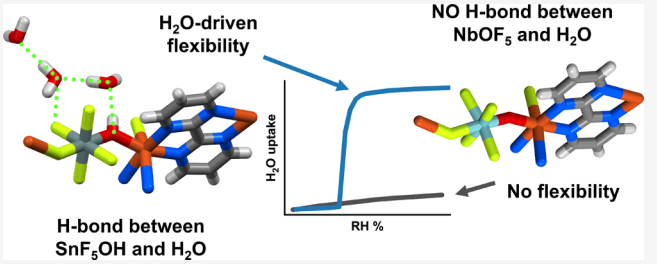

INTRODUCTION

Coordination networks (CNs), including metal−organic frameworks (MOFs),[1] coordination polymers (CPs),[2] and hybrid ultramicroporous materials (HUMs)[3] offer potential to reduce the energy footprints of industrial applications including natural gas storage,[4,5] hydrocarbon separation,[6,7] and atmospheric water harvesting (AWH).[8−10] HUMs, exemplified by the parent HUM, [$Zn(SiF_6)(pyrazine)_2]_n$, **SIFSIX-3-Zn**,[11] feature pores of <7 Å formed by organic linkers and inorganic pillars and can offer benchmark properties for trace CO_2[11,12] or trace hydrocarbon capture.[11,13] Families of HUMs are accessible through inorganic anion substitution, e.g. octahedral MF_6^{2-} or tetrahedral $M'O_4^{2-}$ anions (M = Si, Ti, Sn, Ge; M′ = S, Cr, Mo, respectively), to systematically study structure/property relationships.[14−17] Overall, these studies reveal that combining strong electrostatics with small pore size in HUMs can generate strong and highly selective binding sites for guest molecules.[18−22]

Sn(IV)-based pillars remain underexplored in HUM design, with only 15 examples of structures comprising SnF_6^{2-} anions archived in the Cambridge Structural Database (CSD, Table S1, Figure S1).[22] In addition, HUMs are generally limited to primitive cubic (**pcu**) or square lattice (**sql**) topologies.[14,19,23] HUMs based on MF_6^{2-} anion pillars with diamondoid topology (**dia**), despite being among the earliest[24,25] and most commonly studied topologies in MOFs,[26] are yet to be reported (Figure S2). Another aspect of HUMs which remains understudied concerns guest-induced structural flexibility. When such sorbents switch between closed and open phases, they can offer potential utility for applications including AWH, thanks to the nature of their stepped isotherms which offer enhanced working capacity and thermal regulation.[27,28] Nevertheless, flexible HUMs remain rare with, to the best of our knowledge, only a handful of reported examples: **SIFSIX-23-Cu**[29] and **SIFSIX-23-Cu^N**,[30] **sql-SIFSIX-bpe-Zn**,[23] **sql-**

Received: August 20, 2025
Revised: November 27, 2025
Accepted: December 1, 2025
Published: December 5, 2025

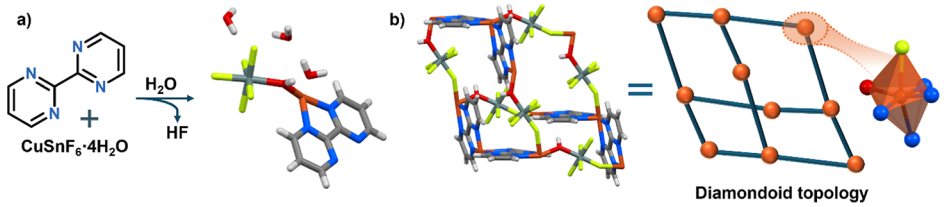

Figure 1. (a) Synthesis of **dia-SNIFFOH-1-Cu**; (b) **dia** topology of **dia-SNIFFOH-1-Cu** and octahedral Cu^{2+} environment. Atom colors: C, gray; N, Blue; O, red; F, neon; Sn, cyan; Cu, orange; H, white.

NbOFFIVE-bpe-Cu,[20] **ZUL-220** or [Cu(4,4′-dipyridylsulfide)$_2$($NbOF_5$)],[31] **GeFSIX-dps-Cu**,[32] and **SIFSIX-dps-Cu**.[33] In this contribution, we report a new flexible HUM comprising a novel anionic pillar, pentafluorohydroxostannate(IV), SnF_5OH^{2-} (**SNIFFOH**), **dia-SNIFFOH-1-Cu**. This is also the first HUM to exhibit **dia** topology. As detailed herein, we also report an investigation of the unusual gas and water vapor sorption properties of **dia-SNIFFOH-1-Cu**.

RESULTS AND DISCUSSION

Hydrothermal reaction of $CuSnF_6{\cdot}4H_2O$ and 2,2′-bipyrimidine (2,2-bimp) afforded blue polyhedral crystals of **dia-SNIFFOH-1-Cu-*α*** (Figure 1a). Bulk synthesis was subsequently conducted through room temperature water slurry (Figure S3). The crystals adopted the monoclinic space group *Cc* (Table S3) and single crystal X-ray crystallography revealed that **dia-SNIFFOH-1-Cu-*α*** is comprised of 4-connected Cu(II) cations linked by chelating 2,2′-bipm ligands and **SNIFFOH** anions to form a noninterpenetrated diamondoid (**dia**) topology coordination network. Three water molecules of hydration were observed per formula unit (Figure 1a). The identity of **SNIFFOH** was unexpected and verified by examination of the Fourier difference map (Figure S4) and X-ray photoelectron spectroscopy (XPS). XPS experiments revealed shoulder peaks around 486.55 and 932.06 eV corresponding to Sn−OH and Cu−OH, respectively, which are present for **dia-SNIFFOH-1-Cu-*α*** but not $CuSnF_6{\cdot}4H_2O$ (Figures 2, S5 and S6). That SnF_6^{2-} had transformed to **SNIFFOH** is consistent with reports on $SnF_{6-n}(OH)_n^{2-}$ (where n = 0−3) anions by Evans et al. in 1968, where ^{19}F NMR spectroscopy was used to study base hydrolysis reactions.[34] To our knowledge, there are no previous reports of SnF_5OH^{2-} serving as a ligand,[22] and its incorporation into **dia-SNIFFOH-1-Cu** affords the first HUM with **dia** topology, enabled by the angular SNIFFOH pillar and 4-connected 2,2-bimp ligand, thereby distinguishing it from **sql** or **pcu** topology HUMS.

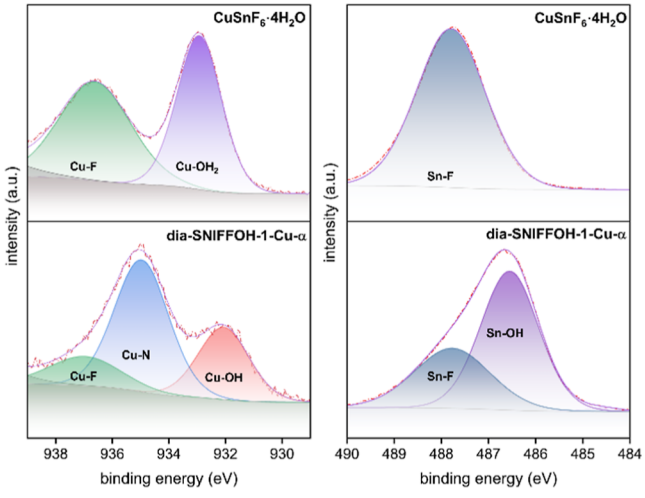

Figure 2. High resolution XPS spectra of **dia-SNIFFOH-1-Cu** and $CuSnF_6{\cdot}4H_2O$ zoomed in to Cu 2p and Sn 3d regions.

The Cu(II) cations in **dia-SNIFFOH-1-Cu-*α*** display Jahn−Teller distortion (Figures 3a, S7 and Table S3) with elongated axial bonds (Cu−F = 2.4191(17) Å, Cu−N = 2.357(2) Å) and equatorial Cu−N bond distances of 2.022(2), 2.036(2), and 2.052(2) Å. The remaining Cu−O bond is *cis* to the fluoro ligand with a bond length of 1.930(2) Å (Figure 3a). The **SNIFFOH** hydroxo moiety and adsorbed water molecules form a hydrogen bonded network that occupies 15.7% void space as calculated by Mercury[35] (Figure 3a). The OH···O hydrogen bond distance between the SNIFFOH anion and a water molecule of hydration is 2.655(3) Å (Figure S8). This water molecule in turn forms H-bonds with a fluoro moiety (F4, 2.705(3) Å) and an adjacent water molecule (O3, 2.669(4) Å) that bonds to a different fluoro moiety (F2, 2.810(3) Å) and the third water molecule (O4, 2.808(4) Å). O4 also forms hydrogen bonds to two fluoro moieties (F5, 2.753(4) Å; F4, 2.799(4) Å).

Thermogravimetric analysis (TGA) and differential scanning calorimetry (DSC) of **dia-SNIFFOH-1-Cu-*α*** revealed 10.53 weight % (wt %) loss between RT and 50 °C corresponding to dehydration (10.67% expected, Figures S9 and S10). DSC showed that this transformation required 318.6 J/g, (54.5 kJ/mol of H_2O, Figure S11).

The crystal structure of **dia-SNIFFOH-1-Cu-*β*** was determined by heating a crystal of **dia-SNIFFOH-1-Cu-*α*** to 333 K under dry N_2, the structural transformation being accompanied by a change in opacity from transparent to opaque (Figures 3a−d and S12). Although the ***α*** to ***β*** transformation did not induce a change in space group (*Cc*, Table S2), the unit cell volume was reduced by 13.1% and the ***β*** phase was found to be nonporous (void space = 0% from Mercury). Bond lengths in the coordination sphere of the ***β*** phase are shorter than the ***α*** phase (Cu−F: 2.26(5) Å, axial Cu−N: 2.270(8) Å; Figure 3d) and the Cu−O−Cu angle is more obtuse (150.16° in ***β*** vs 142.62° in ***α***). This reduced the dimensions of the adamantoid cages of the **dia topology** (20.996 to 20.624 Å) and decreased Cu−Cu layer spacing (10.6123 to 8.823 Å), eliminating porosity (15.7 to 0%; Figures 3e and S13−S15). Variable temperature PXRD (VTPXRD) revealed that water loss was accompanied by phase transformation to **dia-SNIFFOH-1-Cu-*β*** at 40 °C. The ***β*** phase was retained under ambient N_2 flow but exposure to air resulted in reversion to the ***α*** phase (Figure 3f).

The response of **dia-SNIFFOH-1-Cu** to water vapor was further studied through dynamic vapor sorption (DVS). The powdered material was sieved to 50−100 μm particle size

https://doi.org/10.1021/jacs.5c14477
J. Am. Chem. Soc. 2025, 147, 46145−46151

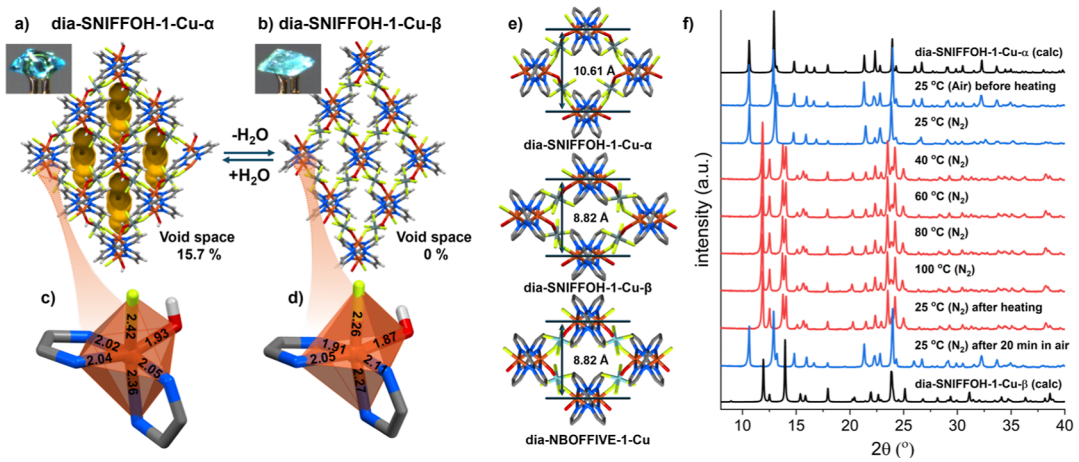

Figure 3. Structural transformation of **dia-SNIFFOH-1-Cu**. Packing of (a) **dia-SNIFFOH-1-Cu-*α*** and (b) **dia-SNIFFOH-1-Cu-*β*** along *c*-axis and single crystal used. Cu^{2+} environment of (c) **dia-SNIFFOH-1-Cu-*α*** and (d) **dia-SNIFFOH-1-Cu-*β***. (e) Cu−Cu distances in **dia-SNIFFOH-1-Cu-*α***, **dia-SNIFFOH-1-Cu-*β***, and **dia-NBOFFIVE-1-Cu**. (f) VTPXRD patterns starting from **dia-SNIFFOH-1-Cu-*α*** (calc = calculated, anhydrate = red, hydrate = blue).

range and heated to 40 °C under a dry air stream to form **dia-SNIFFOH-1-Cu-*β*** in situ (Figures 4a and S16). **dia-SNIFFOH-1-Cu-*β*** displayed an *S*-shaped isotherm with an inflection point at 10.4% RH for a total uptake of 11.95 wt % (313.0 cm^3/cm^3), with desorption occurring with small hysteresis at 5.8% RH. For a 5 mg sample, kinetic measurements revealed that the material reached full loading in 12 min at 30% RH, and 5.7 min at 60% RH, with full desorption taking ∼28.5 min under both conditions (Figure 4b). The sorbent was subjected to 50 humidity swing cycles to evaluate recyclability. No loss of sorption properties occurred and the before and after PXRD patterns matched (Figures 4c and S17 and S18).

As global water scarcity intensifies,[36] AWH is emerging as a potential solution. CNs capable of water adsorption under arid conditions, including **Al-fumarate**,[37] **ROS-039**,[10] and **MOF-303**,[38] are of interest as an alternative to commercial desiccants like **Zeolite 13X** and **Syloid Al-1** because they can be recycled under milder conditions. Key requirements for AWH sorbents include an *S*-shaped isotherm with an inflection below 30% RH, little or no hysteresis, a relatively low regeneration temperature, hydrolytic/mechanical stability over many cycles, fast kinetics, and high productivity (typically measured in kg $_{H_2O}$/kg $_{sorbent}$/day).

Our group has identified that a key criterion for fast sorption kinetics is the difference between the RH of the flow and the RH of the inflection point(s) in the corresponding water vapor isotherm of the sorbent. A desiccant with a low RH inflection point results in faster uptake. Conversely, a desiccant with high RH inflection point results in faster desorption. Temperature swing can be exploited to further increase the rate of desorption.[10]

To evaluate the temperature swing productivity of **dia-SNIFFOH-1-Cu**, four different sample masses (5−15 mg) of sieved 50−100 μm particles were used to measure adsorption−desorption kinetics (Figures S19−S30). These measurements included adsorption at 27 °C, 30% RH (representing loading conditions) and desorption at 60 °C, 5.4% RH (representing unloading conditions). We also collected the sorption isotherm at 60 °C (Figure S31). Furthermore, 11 cycles of temperature swing under the same conditions ([30% RH, 27 °C] − [5.4% RH, 60 °C]) were performed on a 5 mg sample with no loss of performance (Figure S32). Using the underlying diffusion-to-the-bed kinetics model, the gravimetric or volumetric productivity of adsorption/desorption cycling in the AWH process can be predicted using "heatmaps".[10] **dia-SNIFFOH-1-Cu** was thereby compared to the following AWH desiccants: **ROS-037, ROS-039, ROS-040, MIL-160, MOF-303, CAU-10-H** and micronized silica gel (**Syloid**) (Figure S33). The calculated 95th-percentile gravimetric productivity for **dia-SNIFFOH-1-Cu** was found to be 0.31 wt %/min, or 4.52 $kg_{H_2O}/kg_{sorbent}$/day, which is comparable to 0.42 and 0.35 wt %/min observed for **MOF-303** and **ROS-039**, respectively (Figure S33 and Table S4). Whereas working capacity data are typically reported gravimetrically, for some AWH systems, such as those based upon desiccant wheels, volumetric uptake becomes relevant as a greater mass of a desiccant with higher bulk density can be incorporated into desiccant wheels, for which sorbent volume is fixed by rotor dimensions. In such systems, volumetric productivity becomes pertinent. **dia-SNIFFOH-1-Cu** offers greater calculated 95th-percentile performance in $kg_{H_2O}/L_{sorbent}$/day (9.5) than **ROS-040** (8.5), **MIL-160** (8.1), **ROS-039** (7.8), **ROS-037** (6.5), **MOF-303** (6.5), **CAU-10-H** (5.4) and **Syloid** (3.2) (Figures 5a, S34, S35 and Table S4). "Heatmap" analysis can offer insight into how sorption kinetics translate into device-level performance. Under dynamic conditions, the rate of loading is governed by the difference between the RH of the flow and the RH of the inflection step (ΔRH), with low-RH steps enabling faster uptake under arid conditions. These analyses further demonstrate that non-equilibrium cycling at short but realistic times yields higher productivity than equilibrium cycling, a principle that has been validated in real-world AWH systems.[10] The combination of a low-RH step and high volumetric productivity therefore illustrates the potential of **dia-SNIFFOH-1-Cu** as a regeneration-optimized sorbent and highlights design principles relevant to future materials development.

Low-pressure single component gas sorption measurements were conducted using 77 K N_2, 195 K CH_4, CO_2 at 195 and 298 K, as well as C_2 and C_3 hydrocarbons at 298 K on **dia-SNIFFOH-1-Cu**. These experiments revealed negligible

https://doi.org/10.1021/jacs.5c14477
J. Am. Chem. Soc. 2025, 147, 46145−46151

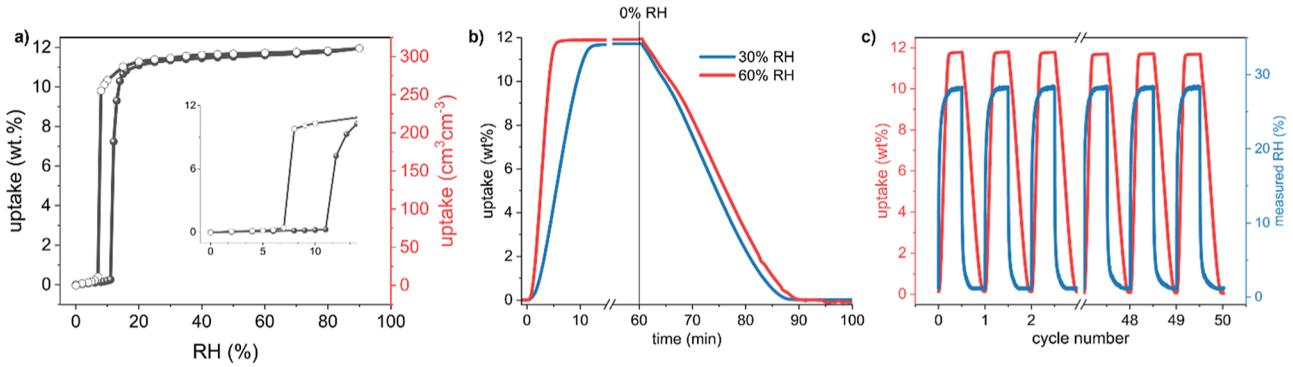

Figure 4. (a) Water vapor sorption isotherm of **dia-SNIFFOH-1-Cu** at 27 °C with an inset image zoomed across 0 to 15%RH (filled and open symbols denote adsorption and desorption points, respectively); (b) kinetics of water vapor adsorption and desorption profiles between 0 to 30% (blue), and 0 to 60% (red); (c) 50 consecutive humidity swing cycles recorded between 0 and 30% RH at 27 °C.

uptake (Figures S36 and S37). We attribute these data to the ultramicroporous nature of the coordination network, which, with a pore limiting diameter of 1.97 Å at 298 K, is well below the kinetic diameters of H_2O (2.65 Å), CO_2 (3.30 Å) and N_2 (3.64 Å).[39] The observation of switching induced by water vapor suggests the possibility of, for example, sieving to enable dehumidification of flue gas streams prior to carbon capture or of natural gas streams. This property was tested through H_2O/CO_2 breakthrough experiments using a moisture-saturated CO_2 stream (Figure 5b). Breakthrough of water vapor was not observed during the adsorption branch of the experiment (0 to 57.14 min/g) whereas breakthrough of CO_2 was observed rapidly, within 1.67 min/g, consistent with the expected negligible CO_2 adsorption, as supported by the absence of a significant CO_2 signal in the temperature-programmed desorption (TPD) phase of the experiment. However, TPD data indicated desorption of a significant amount of water between 90.3 min/g and 315 min/g. This behavior is consistent with gate-opening of **dia-SNIFFOH-1-Cu** upon exposure to the humid CO_2 stream under dynamic conditions and H_2O-over-CO_2 sieving. Building on our recent findings with nonequilibrium CO_2 and H_2O loading in **TIFSIX-3-Ni**,[40] we recognize that achieving a breakthrough front for H_2O would require an impractically long experimental duration, with minimal influence on CO_2 loading in the **dia-SNIFFOH-1-Cu-*β*** bed. While qualitative, the DCB experimental data underscore that sieving of H_2O over CO_2 had occurred. To the best of our knowledge, **dia-SNIFFOH-1-Cu** represents the first CN to exhibit selective H_2O-over-CO_2 sieving in both the ***α*** and ***β*** phases, effectively functioning as a "double sieve."

To further investigate the sieving properties of **dia-SNIFFOH-1-Cu**, NH_3 and He sorption experiments were conducted at 298 K. Both NH_3 and He have smaller kinetic diameters (2.60 Å) than H_2O (2.65 Å). The NH_3 isotherm exhibited a stepped adsorption profile with a saturation uptake of 267 $cm^3\ g^{-1}$, indicating that NH_3 induces switching like H_2O (Figure S38). However, strong hysteresis with incomplete desorption was observed and PXRD analysis of the post-sorption sample revealed loss of crystallinity (Figure S39). These observations, along with the distinct color change observed before and after sorption, suggest chemisorption of NH_3 and loss of structural integrity (Figures S39 and S40). In contrast, He sorption experiments performed at 77 and 298 K revealed negligible uptake (Figures S41 and S42). Despite having a similar kinetic diameter to NH_3, He lacks hydrogen-bonding capability, which may be critical for triggering phase transformation from nonporous to porous. PXRD analysis indicates that **dia-SNIFFOH-1-Cu** had retained crystallinity after He exposure (Figure S43).

A second member of this **dia** topology family, **dia-NBOFFIVE-1-Cu**, was synthesized by reacting $CuNbOF_5 \cdot 4H_2O$ with 2,2′-bipm in water at 60 °C, yielding rod-shaped crystals in the monoclinic *Cc* space group (NBOFFIVE = $NbOF_5^{2-}$; Table S5). Bulk samples, including isostructural Zn, Co, and Ni analogs, were prepared *via* water slurry and characterized by PXRD (Figure S44). Unlike **dia-SNIFFOH-1-Cu-*α***, **dia-NBOFFIVE-1-Cu** is a nonporous anhydrate in its as-synthesized phase. The structure also exhibits positional disorder around the **NBOFFIVE** pillar over two general positions with a 75:25 occupancy ratio (Figure S45). Nevertheless, **dia-NBOFFIVE-1-Cu** has unit cell parameters and volume (V = 1178.52(9)) similar to that of **dia-SNIFFOH-1-Cu-*β***, and the calculated and experimental PXRD patterns are in good agreement (Figure S12). Jahn–Teller distortion leads to elongated axial bonds (Cu–F: 2.219(6) Å; Cu–N: 2.280(5) Å), typical equatorial Cu–N bonds (2.039(5), 2.069(4), 2.016(5) Å) and a Cu–O bond of 1.973(5) Å. This distortion results in a more obtuse Cu–O–Cu angle of 165.79° and a reduced Cu–Cu spacing of 8.82 Å, (compared to 142.62° and 10.61 Å in **dia-SNIFFOH-1-Cu-*α***, Figures 3e, S3, S13–S15). Despite structural similarities to **dia-SNIFFOH-1-Cu-*β***, **dia-NBOFFIVE-1-Cu** features different pore chemistry due to an oxo ligand replacing the hydroxo group. The water sorption isotherm of **dia-NBOFFIVE-1-Cu** revealed uptake of 3 wt %, consistent with surface sorption by a nonporous material (Figure S46).

To better understand the experimental adsorption behavior, we performed hybrid GCMC–MD simulations on **dia-SNIFFOH-1-Cu-*α***, **dia-SNIFFOH-1-Cu-*β*** and **dia-NBOFFIVE-1-Cu** to study CO_2 and H_2O adsorption (for detailed computational methods, see Supporting Information, Figures S47–S50, Tables S6–S12). **H_2O** was found to adsorb only in the porous ***α*** phase of **dia-SNIFFOH-1-Cu**, where the pore structure not only facilitates molecular diffusion but also enables stabilizing interactions, specifically, hydrogen bonding with fluorinated linkers (Figures S48 and S49). In the ***β*** phase and in **dia-NBOFFIVE-1-Cu**, significantly lower free volumes (Table S12) restrict access to potential binding sites, resulting in negligible uptake for H_2O, while **CO_2** does not adsorb in any of the structures, which is suggestive of weaker interactions or sieving. Overall, the GCMC-MD simulations are not only consistent with the key trends observed experimentally (Figure

https://doi.org/10.1021/jacs.5c14477
J. Am. Chem. Soc. 2025, 147, 46145–46151

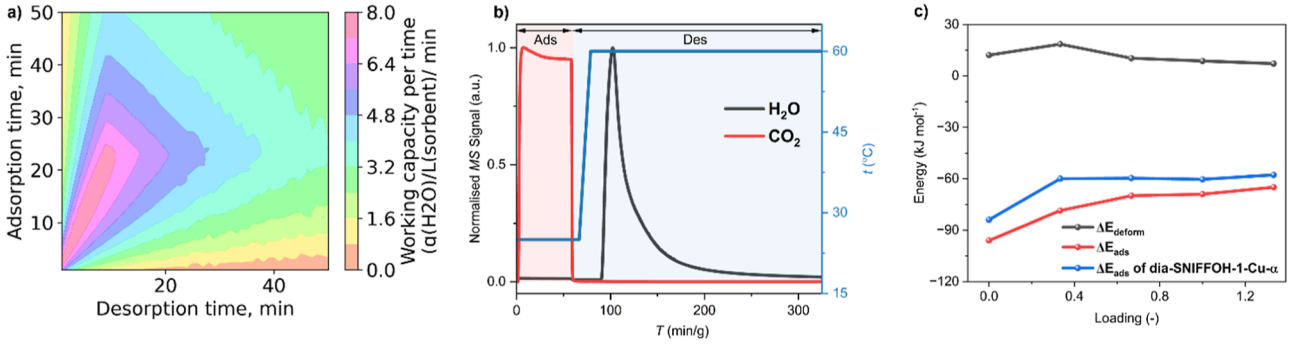

Figure 5. (a) Water vapor sorption productivity "heatmap" of **dia-SNIFFOH-1-Cu** calculated using a diffusion to the bed kinetics model.[10] (b) A comparison of one cycle each of adsorption and temperature-programmed desorption curves for breakthrough of moisture-saturated CO_2 stream at a flow rate of 10 cm^3 min^{-1} (75% RH, 2.25% v/v) (MS = mass spectroscopy). (c) Energy decomposition analysis per adsorbed water molecule (in kJ/mol). $\Delta E_{ads,dia\text{-}SNIFFOH\text{-}1\text{-}Cu\text{-}\alpha} = \Delta E_{deform} + \Delta E_{ads}$. The loading was normalized on the maximum loading observed experimentally of 3 H_2O per Cu-site.

5c), but they also provide molecular-level insight into how pore accessibility and host−guest interactions drive phase-selective adsorption. Moreover, DFT calculations optimizing randomly selected adsorbate-framework configurations revealed the structural flexibility of **dia-SNIFFOH-1-Cu-*α*** to be a function of the sorption process. Interestingly, the framework initially contracts (−1.3%) at low water loading (0.5 H_2O per Cu), and then gradually expands with increasing loading; +2.7% (1 H_2O per Cu), +4.9% (2 H_2O per Cu), +6.1% (3 H_2O per Cu), +7.8% (4 H_2O per Cu). The adsorption energy with respect to pristine **dia-SNIFFOH-1-Cu-*α*** can be deconvoluted into the endothermic framework deformation energy and exothermic water adsorption energy. The deformation penalty typically varies between 7.2 and 18.6 kJ/mol per H_2O, while exothermic adsorption energy decreases from −96 (0.5 H_2O per Cu-site) to −65 kJ/mol (4 H_2O per Cu). As such, water molecules interacting with the pore through hydrogen bonding interactions facilitate structural flexibility.

CONCLUSION

In summary, we report water-mediated synthesis, structural characterization, and sorption properties of the first **dia** topology HUM, which is sustained by a new pillar anion, SnF_5OH^{2-} (**SNIFFOH**). **dia-SNIFFOH-1-Cu** exhibits a reversible, water-induced phase transformation, resulting in an *S*-shaped water sorption isotherm with an inflection point at 10% RH, fast adsorption, desorption below 60 °C, and stability over at least 50 cycles. Computational modeling supports that water sorption occurs exclusively in the open-pore phase driven by exothermic binding in the pore. To our knowledge, **dia-SNIFFOH-1-Cu** represents only the second example of a CN that exhibits a water-induced structural transformation at *ca.* 10% RH after **ZFP-2-Co**.[41] Alongside competitive gravimetric performance (12 wt %), its high density affords a volumetric uptake of 313 cm^3/cm^3, which is advantageous for processes based upon desiccant wheels. The H_2O over CO_2 sieving observed herein not only suggests potential for atmospheric AWH, but also flue gas or natural gas dehumidification. That the inorganic pillar **SNIFFOH** offers very different pore chemistry for water molecule binding than traditional inorganic pillars is key to the observed properties.

ASSOCIATED CONTENT

Supporting Information

The Supporting Information is available free of charge at https://pubs.acs.org/doi/10.1021/jacs.5c14477.

Additional experimental details and methods, including TGA, sorption isotherms, PXRD, and DSC are included in the Supporting Information (PDF). Crystallographic data can be accessed from the Cambridge Crystallographic Data Centre (CCDC) as deposition entries 2403362−2403368 (PDF)

Accession Codes

Deposition Numbers 2403362−2403368 contain the supplementary crystallographic data for this paper. These data can be obtained free of charge via the joint Cambridge Crystallographic Data Centre (CCDC) and Fachinformationszentrum Karlsruhe Access Structures service.

AUTHOR INFORMATION

Corresponding Author

Michael J. Zaworotko − *Department of Chemical Sciences and Bernal Institute, University of Limerick, Limerick V94 T9PX, Ireland;* orcid.org/0000-0002-1360-540X; Email: Xtal@ul.ie.

Authors

Yassin H Andaloussi − *Department of Chemical Sciences and Bernal Institute, University of Limerick, Limerick V94 T9PX, Ireland*

Aizhamal Subanbekova − *Department of Chemical Sciences and Bernal Institute, University of Limerick, Limerick V94 T9PX, Ireland;* orcid.org/0009-0008-4254-0749

Kyriaki Koupepidou − *Institute for Integrated Cell-Material Sciences (iCeMS), Kyoto University Institute for Advanced Study (KUIAS), Kyoto 606-8501, Japan;* orcid.org/0000-0001-6934-3261

Sousa Javan Nikkhah − *Department of Chemical Sciences and Bernal Institute, University of Limerick, Limerick V94 T9PX, Ireland; Department of Chemistry and Kathleen Lonsdale Institute, Maynooth University, Maynooth W23 F2H6, Ireland;* orcid.org/0000-0003-1725-4069

Andrey A. Bezrukov − *Department of Chemical Sciences and Bernal Institute, University of Limerick, Limerick V94 T9PX, Ireland;* orcid.org/0000-0002-0525-3547

Asif Raza − *Department of Chemical Sciences and Bernal Institute, University of Limerick, Limerick V94 T9PX, Ireland*
Hirotoshi Sakamoto − *Institute for Integrated Cell-Material Sciences (iCeMS), Kyoto University Institute for Advanced Study (KUIAS), Kyoto 606-8501, Japan;* orcid.org/0000-0002-0873-1321
Susumu Kitagawa − *Institute for Integrated Cell-Material Sciences (iCeMS), Kyoto University Institute for Advanced Study (KUIAS), Kyoto 606-8501, Japan;* orcid.org/0000-0001-6956-9543
Matthias Vandichel − *Department of Chemical Sciences and Bernal Institute, University of Limerick, Limerick V94 T9PX, Ireland;* orcid.org/0000-0003-1592-0726
Soumya Mukherjee − *Department of Chemical Sciences and Bernal Institute, University of Limerick, Limerick V94 T9PX, Ireland;* orcid.org/0000-0003-2375-7009

Complete contact information is available at: https://pubs.acs.org/10.1021/jacs.5c14477

Author Contributions

[‖]Y.H.A. and A.S. contributed equally to this work. All authors have given approval to the final version of the manuscript.

Notes

The authors declare no competing financial interest.

■ ACKNOWLEDGMENTS

M.J.Z. acknowledges support from the European Research Council (ADG 885695) and Research Ireland (16/IA/4624, IRCLA/2019/167). S.M. acknowledges Research Ireland (21/PATH-S/9454) and SSPC (the Research Ireland Centre for Pharmaceuticals, 12/RC/2275_P2) for research funding. K.K. thanks the Japan Society of the Promotion of Science (JSPS) under the JSPS Postdoctoral Fellowship for Research in Japan programme (ID: PE24049). K.K., H.S. and S.K. acknowledge the financial support of KAKENHI, Grant-in-Aid for Scientific Research (22H05005, 23K26668). S.J.N. and M.V. acknowledge Research Ireland (23/FFP-A/12221). The authors also thank the iCeMS Analysis Centre for access to analytical instruments.

■ ABBREVIATIONS

CCDC, Cambridge Crystallographic Data Center; CN, coordination network; CP, coordination polymer; DCB, dynamic column breakthrough; **dia**, diamondoid; DSC, differential scanning calorimetry; DVS, dynamic vapor sorption; HUM, hybrid ultramicroporous material; MOF, metal−organic framework; MS, mass spectroscopy; **pcu**, primitive cubic; PXRD, powder X-ray diffractometry; RH, relative humidity; SC−SC, single-crystal-to-single-crystal; SCXRD, single crystal X-ray diffractometry; **sql**, square lattice; TGA, thermogravimetric analysis; TPD, temperature-programmed desorption; XPS, X-ray photoelectron spectroscopy; GCMC−MD, grand canonical monte carlo−molecular dynamics; DFT, density functional theory.

■ REFERENCES

(1) Furukawa, H.; Cordova, K. E.; O'Keeffe, M.; Yaghi, O. M. The chemistry and applications of metal-organic frameworks. *Science* **2013**, *341* (6149), 1230444.
(2) Kitagawa, S.; Kitaura, R.; Noro, S. i. Functional porous coordination polymers. *Angew. Chem., Int. Ed.* **2004**, *43* (18), 2334−2375.
(3) Mukherjee, S.; Zaworotko, M. J. Crystal Engineering of Hybrid Coordination Networks: From Form to Function. *Trends Chem. Chem.* **2020**, *2* (6), 506−518.
(4) Sanz-Pérez, E. S.; Murdock, C. R.; Didas, S. A.; Jones, C. W. Direct capture of CO2 from ambient air. *Chem. Rev.* **2016**, *116* (19), 11840−11876.
(5) Osman, A. I.; Hefny, M.; Abdel Maksoud, M.; Elgarahy, A. M.; Rooney, D. W. Recent advances in carbon capture storage and utilisation technologies: a review. *Environ. Chem. Lett.* **2021**, *19* (2), 797−849.
(6) Mukherjee, S.; Sensharma, D.; Chen, K.-J.; Zaworotko, M. J. Crystal engineering of porous coordination networks to enable separation of C2 hydrocarbons. *Chem. Commun.* **2020**, *56* (72), 10419−10441.
(7) Yang, L.; Zhang, P.; Cui, J.; Cui, X.; Xing, H. The Chemistry of Metal−Organic Frameworks for Multicomponent Gas Separation. *Angew. Chem., Int. Ed.* **2024**, *63* (46), No. e202414503.
(8) Hanikel, N.; Prévot, M. S.; Yaghi, O. M. MOF water harvesters. *Nat. Nanotechnol.* **2020**, *15* (5), 348−355.
(9) Bilal, M.; Sultan, M.; Morosuk, T.; Den, W.; Sajjad, U.; Aslam, M. M.; Shahzad, M. W.; Farooq, M. Adsorption-based atmospheric water harvesting: A review of adsorbents and systems. *Int. Commun. Heat Mass Transfer* **2022**, *133*, 105961.
(10) Bezrukov, A. A.; O'Hearn, D. J.; Gascón-Pérez, V.; Darwish, S.; Kumar, A.; Sanda, S.; Kumar, N.; Francis, K.; Zaworotko, M. J. Metal-organic frameworks as regeneration optimized sorbents for atmospheric water harvesting. *Cell Rep. Phys. Sci.* **2023**, *4* (2), 101252.
(11) Nugent, P.; Belmabkhout, Y.; Burd, S. D.; Cairns, A. J.; Luebke, R.; Forrest, K.; Pham, T.; Ma, S.; Space, B.; Wojtas, L.; et al. Porous materials with optimal adsorption thermodynamics and kinetics for CO2 separation. *Nature* **2013**, *495* (7439), 80−84.
(12) Shekhah, O.; Belmabkhout, Y.; Chen, Z.; Guillerm, V.; Cairns, A.; Adil, K.; Eddaoudi, M. Made-to-order metal-organic frameworks for trace carbon dioxide removal and air capture. *Nat. Commun.* **2014**, *5* (1), 4228.
(13) Cui, X.; Chen, K.; Xing, H.; Yang, Q.; Krishna, R.; Bao, Z.; Wu, H.; Zhou, W.; Dong, X.; Han, Y.; et al. Pore chemistry and size control in hybrid porous materials for acetylene capture from ethylene. *Science* **2016**, *353* (6295), 141−144.
(14) Sensharma, D.; O'Hearn, D. J.; Koochaki, A.; Bezrukov, A. A.; Kumar, N.; Wilson, B. H.; Vandichel, M.; Zaworotko, M. J. The First Sulfate-Pillared Hybrid Ultramicroporous Material, SOFOUR-1-Zn, and Its Acetylene Capture Properties. *Angew. Chem., Int. Ed.* **2022**, *61* (8), No. e202116145.
(15) Mohamed, M. H.; Elsaidi, S. K.; Pham, T.; Forrest, K. A.; Tudor, B.; Wojtas, L.; Space, B.; Zaworotko, M. J. Pillar substitution modulates CO2 affinity in "mmo" topology networks. *Chem. Commun.* **2013**, *49* (84), 9809−9811.
(16) Sensharma, D.; Wilson, B. H.; Kumar, N.; O'Hearn, D. J.; Zaworotko, M. J. Pillar modularity in fsc topology hybrid ultramicroporous materials based upon tetra (4-pyridyl) benzene. *Cryst. Growth Des.* **2022**, *22* (9), 5472−5480.
(17) Harvey-Reid, N. C.; Sensharma, D.; Mukherjee, S.; Patil, K. M.; Kumar, N.; Nikkhah, S. J.; Vandichel, M.; Zaworotko, M. J.; Kruger, P. E. Crystal Engineering of a New Hexafluorogermanate Pillared Hybrid Ultramicroporous Material Delivers Enhanced Acetylene Selectivity. *ACS Appl. Mater. Interfaces* **2024**, *16* (4), 4803−4810.
(18) Liu, X.; Zhang, P.; Xiong, H.; Zhang, Y.; Wu, K.; Liu, J.; Krishna, R.; Chen, J.; Chen, S.; Zeng, Z.; et al. Engineering Pore Environments of Sulfate-Pillared Metal-Organic Framework for Efficient C2H2/CO2 Separation with Record Selectivity. *Adv. Mater.* **2023**, *35* (20), 2210415.
(19) Zhang, Y.; Sun, W.; Luan, B.; Li, J.; Luo, D.; Jiang, Y.; Wang, L.; Chen, B. Topological Design of Unprecedented Metal-Organic Frameworks Featuring Multiple Anion Functionalities and Hierarchical Porosity for Benchmark Acetylene Separation. *Angew. Chem., Int. Ed.* **2023**, *62* (3), No. e202309925.
(20) Gao, M.-Y.; Bezrukov, A. A.; Song, B.-Q.; He, M.; Nikkhah, S. J.; Wang, S.-Q.; Kumar, N.; Darwish, S.; Sensharma, D.; Deng, C.;

et al. Highly Productive C3H4/C3H6 Trace Separation by a Packing Polymorph of a Layered Hybrid Ultramicroporous Material. *J. Am. Chem. Soc.* **2023**, *145* (21), 11837−11845.
(21) Ebadi Amooghin, A.; Sanaeepur, H.; Luque, R.; Garcia, H.; Chen, B. Fluorinated metal−organic frameworks for gas separation. *Chem. Soc. Rev.* **2022**, *51* (17), 7427−7508.
(22) Groom, C. R.; Bruno, I. J.; Lightfoot, M. P.; Ward, S. C. The Cambridge structural database. *Struct. Sci.* **2016**, *72* (2), 171−179.
(23) Shivanna, M.; Otake, K. i.; Song, B. Q.; van Wyk, L. M.; Yang, Q. Y.; Kumar, N.; Feldmann, W. K.; Pham, T.; Suepaul, S.; Space, B.; et al. Benchmark acetylene binding affinity and separation through induced fit in a flexible hybrid ultramicroporous material. *Angew. Chem., Int. Ed.* **2021**, *60* (37), 20383−20390.
(24) Zaworotko, M. J. Crystal engineering of diamondoid networks. *Chem. Soc. Rev.* **1994**, *23* (4), 283−288.
(25) Hoskins, B. F.; Robson, R. Design and construction of a new class of scaffolding-like materials comprising infinite polymeric frameworks of 3D-linked molecular rods. A reappraisal of the zinc cyanide and cadmium cyanide structures and the synthesis and structure of the diamond-related frameworks [N (CH3) 4][CuIZnII (CN) 4] and CuI [4, 4', 4'', 4'''-tetracyanotetraphenylmethane] BF4. xC6H5NO2. *J. Am. Chem. Soc.* **1990**, *112* (4), 1546−1554.
(26) Alexandrov, E. V.; Blatov, V. A.; Kochetkov, A. V.; Proserpio, D. M. Underlying nets in three-periodic coordination polymers: topology, taxonomy and prediction from a computer-aided analysis of the Cambridge Structural Database. *CrystEngComm* **2011**, *13* (12), 3947−3958.
(27) Li, X.; Bian, H.; Huang, W.; Yan, B.; Wang, X.; Zhu, B. A review on anion-pillared metal−organic frameworks (APMOFs) and their composites with the balance of adsorption capacity and separation selectivity for efficient gas separation. *Coord. Chem. Rev.* **2022**, *470*, 214714.
(28) Koupepidou, K.; Subanbekova, A.; Zaworotko, M. J. Functional flexible adsorbents and their potential utility. *Chem. Commun.* **2025**, *61* (15), 3109−3126.
(29) Song, B.-Q.; Yang, Q.-Y.; Wang, S.-Q.; Vandichel, M.; Kumar, A.; Crowley, C.; Kumar, N.; Deng, C.-H.; GasconPerez, V.; Lusi, M.; et al. Reversible switching between nonporous and porous phases of a new SIFSIX coordination network induced by a flexible linker ligand. *J. Am. Chem. Soc.* **2020**, *142* (15), 6896−6901.
(30) Song, B. Q.; Shivanna, M.; Gao, M. Y.; Wang, S. Q.; Deng, C. H.; Yang, Q. Y.; Nikkhah, S. J.; Vandichel, M.; Kitagawa, S.; Zaworotko, M. J. Shape-Memory Effect Enabled by Ligand Substitution and CO2 Affinity in a Flexible SIFSIX Coordination Network. *Angew. Chem., Int. Ed.* **2023**, *62* (47), No. e202309985.
(31) Shen, J.; He, X.; Ke, T.; Krishna, R.; van Baten, J. M.; Chen, R.; Bao, Z.; Xing, H.; Dincă, M.; Zhang, Z.; et al. Simultaneous interlayer and intralayer space control in two-dimensional metal− organic frameworks for acetylene/ethylene separation. *Nat. Commun.* **2020**, *11* (1), 6259.
(32) Ke, T.; Wang, Q.; Shen, J.; Zhou, J.; Bao, Z.; Yang, Q.; Ren, Q. Molecular Sieving of C2-C3 Alkene from Alkyne with Tuned Threshold Pressure in Robust Layered Metal−Organic Frameworks. *Angew. Chem., Int. Ed.* **2020**, *59* (31), 12725−12730.
(33) Wang, J.; Zhang, Y.; Su, Y.; Liu, X.; Zhang, P.; Lin, R.-B.; Chen, S.; Deng, Q.; Zeng, Z.; Deng, S.; et al. Fine pore engineering in a series of isoreticular metal-organic frameworks for efficient C2H2/CO2 separation. *Nat. Commun.* **2022**, *13* (1), 200.
(34) Dean, P. A. W.; Evans, D. F. Spectroscopic studies of inorganic fluoro-complexes. Part II. 19F nuclear magnetic resonance studies of tin(IV) fluoro-complexes. *J. Chem. Soc. Inorg. Phys. Theor.* **1968**, No. 0, 1154−1166.
(35) Macrae, C. F.; Sovago, I.; Cottrell, S. J.; Galek, P. T.; McCabe, P.; Pidcock, E.; Platings, M.; Shields, G. P.; Stevens, J. S.; Towler, M.; et al. Mercury 4.0: From visualization to analysis, design and prediction. *J. Appl. Crystallogr.* **2020**, *53* (1), 226−235.
(36) Wang, M.; Bodirsky, B. L.; Rijneveld, R.; Beier, F.; Bak, M. P.; Batool, M.; Droppers, B.; Popp, A.; van Vliet, M. T.; Strokal, M. A triple increase in global river basins with water scarcity due to future pollution. *Nat. Commun.* **2024**, *15* (1), 880.
(37) Jeremias, F.; Fröhlich, D.; Janiak, C.; Henninger, S. K. Advancement of sorption-based heat transformation by a metal coating of highly-stable, hydrophilic aluminium fumarate MOF. *RSC Adv.* **2014**, *4* (46), 24073−24082.
(38) Hanikel, N.; Prévot, M. S.; Fathieh, F.; Kapustin, E. A.; Lyu, H.; Wang, H.; Diercks, N. J.; Glover, T. G.; Yaghi, O. M. Rapid Cycling and Exceptional Yield in a Metal-Organic Framework Water Harvester. *ACS Cent. Sci.* **2019**, *5* (10), 1699−1706.
(39) Fauzi, A.; Kailash, I.; Khulbe, C.; Matsuura, T. *Gas Separation Membranes: Polymeric and Inorganic*; Springer: Cham, Switzerland, 2015.
(40) Ullah, S.; Tan, K.; Sensharma, D.; Kumar, N.; Mukherjee, S.; Bezrukov, A. A.; Li, J.; Zaworotko, M. J.; Thonhauser, T. CO2 Capture by Hybrid Ultramicroporous TIFSIX-3-Ni under Humid Conditions Using Non-Equilibrium Cycling. *Angew. Chem., Int. Ed.* **2022**, *61* (35), No. e202206613.
(41) Yang, M.; Wang, S.-Q.; Liu, Z.; Chen, Y.; Zaworotko, M. J.; Cheng, P.; Ma, J.-G.; Zhang, Z. Fabrication of Moisture-Responsive Crystalline Smart Materials for Water Harvesting and Electricity Transduction. *J. Am. Chem. Soc.* **2021**, *143* (20), 7732−7739.

https://doi.org/10.1021/jacs.5c14477
J. Am. Chem. Soc. 2025, 147, 46145−46151